Mon. Not. R. Astron. Soc. **000**, 1–10 (0000) Printed 5 July 2010 (MN LATEX style file v2.2)

Further X-ray observations of EXO 0748–676 in quiescence: evidence for a cooling neutron star crust

N. Degenaar[1⋆], M.T. Wolff[2], P.S. Ray[2], K.S. Wood[2], J. Homan[3], W.H.G. Lewin[3], P.G. Jonker[4,5], E.M. Cackett[6], J.M. Miller[6], E.F. Brown[7], R. Wijnands[1]
[1] *Astronomical Institute "Anton Pannekoek", University of Amsterdam, Science Park 904, 1098 XH, Amsterdam, the Netherlands*
[2] *Space Science Division, Naval Research Laboratory, Washington, DC 20375, USA*
[3] *MIT Kavli Institute for Astrophysics and Space Research, 70 Vassar Street, Cambridge, MA 02139, USA*
[4] *SRON, Netherlands Institute for Space Research, Sorbonnelaan 2, 3584 CA, Utrecht, the Netherlands*
[5] *Harvard-Smithsonian Center for Astrophysics, 60 Garden Street, Cambridge, MA 02138, U.S.A.*
[6] *Chandra fellow, University of Michigan, Department of Astronomy, 500 Church Street, Dennison 814, Ann Arbor, MI 48105, USA*
[7] *Department of Physics and Astronomy, Michigan State University, East Lansing, MI 48824, USA*

Received XXXX / Accepted XXXX / DRAFT VERSION

ABSTRACT
In late 2008, the quasi-persistent neutron star X-ray transient and eclipsing binary EXO 0748–676 started a transition from outburst to quiescence, after it had been actively accreting for more than 24 years. In a previous work, we discussed *Chandra* and *Swift* observations obtained during the first five months after this transition. Here, we report on further X-ray observations of EXO 0748–676, extending the quiescent monitoring to 1.6 years. *Chandra* and *XMM-Newton* data reveal quiescent X-ray spectra composed of a soft, thermal component that is well-fitted by a neutron star atmosphere model. An additional hard powerlaw tail is detected that changes non-monotonically over time, contributing between 4 and 20 percent to the total unabsorbed 0.5–10 keV flux. The combined set of *Chandra*, *XMM-Newton* and *Swift* data reveals that the thermal bolometric luminosity fades from $\sim 1 \times 10^{34}$ to 6×10^{33} (d/7.4 kpc)^2 erg s^{-1}, whereas the inferred neutron star effective temperature decreases from $\sim$ 124 to 109 eV. We interpret the observed decay as cooling of the neutron star crust and show that that the quiescent lightcurve of EXO 0748–676 is markedly shallower than that observed for three other neutron star X-ray binaries that underwent prolonged accretion outbursts.

Key words: accretion, accretion disks - binaries: eclipsing - stars: individual (EXO 0748–676) - stars: neutron - X-rays: binaries

1 INTRODUCTION

EXO 0748–676 is an intensively studied low-mass X-ray binary that was initially discovered with the European X-ray Observatory SATellite (*EXOSAT*) in 1985 February (Parmar et al. 1985). In retrospect the source already appeared active in *EXOSAT* slew survey observations several times beginning 1984 July (Reynolds et al. 1999). The detection of type-I X-ray bursts (e.g., Gottwald et al. 1986) identify the compact primary as a neutron star. A few X-ray bursts have been observed that exhibited photospheric radius expansion, which allows for a distance estimate towards the source of $D = 5.0 - 8.3$ kpc, depending on the composition of the photosphere (Wolff et al. 2005; Galloway et al. 2008). The system exhibits irregular X-ray dips and displays eclipses that last for $\sim$ 8.3 min and recur every 3.82 hr, which allow the unambiguous determination of the orbital period of the binary (Parmar et al. 1986; Wolff et al. 2009).

At the time of its discovery, EXO 0748–676 was detected at 2–10 keV luminosities of $\sim (1 - 7) \times 10^{36}$ (D/7.4 kpc)^2 erg s^{-1} (Parmar et al. 1986). However, several years prior to the *EXOSAT* detections, it was serendipitously observed with the *EINSTEIN* satellite in 1980 May, displaying a 0.5–10 keV luminosity of $\sim 5 \times 10^{33}$ (D/7.4 kpc)^2 erg s^{-1} (Parmar et al. 1986; Garcia & Callanan 1999). The source can thus be classified as a transient X-ray binary. Nevertheless, such systems typically exhibit accretion outbursts that last only weeks to months (e.g., Chen et al. 1997), whereas EXO 0748–676 was persistently detected at luminosities of $\sim 10^{36-37}$ (D/7.4 kpc)^2 erg s^{-1} by various satellites for over 24 years. Similar prolonged accretion episodes continuing

⋆ e-mail: degenaar@uva.nl

Report Documentation Page

Form Approved
OMB No. 0704-0188

1. REPORT DATE	2. REPORT TYPE	3. DATES COVERED
JUL 2010		**00-00-2010 to 00-00-2010**

4. TITLE AND SUBTITLE	5a. CONTRACT NUMBER
Further X-ray observations of EXO 0748-676 in quiescence: evidence for a cooling neutron star crust	5b. GRANT NUMBER
	5c. PROGRAM ELEMENT NUMBER
6. AUTHOR(S)	5d. PROJECT NUMBER
	5e. TASK NUMBER
	5f. WORK UNIT NUMBER
7. PERFORMING ORGANIZATION NAME(S) AND ADDRESS(ES) **Naval Research Laboratory,Space Science Division,Washington,DC,20375**	8. PERFORMING ORGANIZATION REPORT NUMBER
9. SPONSORING/MONITORING AGENCY NAME(S) AND ADDRESS(ES)	10. SPONSOR/MONITOR'S ACRONYM(S)
	11. SPONSOR/MONITOR'S REPORT NUMBER(S)

12. DISTRIBUTION/AVAILABILITY STATEMENT
Approved for public release; distribution unlimited

13. SUPPLEMENTARY NOTES

14. ABSTRACT

In late 2008, the quasi-persistent neutron star X-ray transient and eclipsing binary EXO 0748?676 started a transition from outburst to quiescence, after it had been actively accreting for more than 24 years. In a previous work, we discussed Chandra and Swift observations obtained during the first five months after this tran- sition. Here, we report on further X-ray observations of EXO 0748?676, extending the quiescent monitoring to 1.6 years. Chandra and XMM-Newton data reveal qui- escent X-ray spectra composed of a soft, thermal component that is well-fitted by a neutron star atmosphere model. An additional hard powerlaw tail is detected that changes non-monotonically over time, contributing between 4 and 20 percent to the total unabsorbed 0.5?10 keV flux. The combined set of Chandra, XMM-Newton and Swift data reveals that the thermal bolometric luminosity fades from 1 ?1034 to 6?033 (d/7.4 kpc)2 erg s−1, whereas the inferred neutron star effective temperature decreases from 124 to 109 eV. We interpret the observed decay as cooling of the neutron star crust and show that that the quiescent lightcurve of EXO 0748?676 is markedly shallower than that observed for three other neutron star X-ray binaries that underwent prolonged accretion outbursts.

15. SUBJECT TERMS

16. SECURITY CLASSIFICATION OF:			17. LIMITATION OF ABSTRACT	18. NUMBER OF PAGES	19a. NAME OF RESPONSIBLE PERSON
a. REPORT **unclassified**	b. ABSTRACT **unclassified**	c. THIS PAGE **unclassified**	**Same as Report (SAR)**	**10**	

for years to decades have been observed for a few other systems, which are termed quasi-persistent X-ray binaries (e.g., Wijnands 2004).

In 2008 August–September, observations with the Proportional Counter Array (PCA) onboard the *Rossi X-ray Timing Explorer* (*RXTE*) and *Swift*'s X-ray Telescope (XRT) indicated that the X-ray flux of EXO 0748–676 was declining (Wolff et al. 2008a,b). Optical and near-IR observations of the optical counterpart, UY Vol, performed in 2008 October showed that the optical emission had also faded compared to the brighter X-ray state (Hynes & Jones 2008, 2009; Torres et al. 2008). These events indicated that the accretion was ceasing and that the system was transitioning from outburst to quiescence. This is also illustrated by Fig. 1, which displays the X-ray lightcurve of EXO 0748–676 as observed with the All-Sky Monitor (ASM) onboard *RXTE* since 1996. The decrease in source activity is clearly seen around ~ 4600 days.

Chandra observations carried out in 2008 mid-October (i.e., after the transition to quiescence) revealed an X-ray spectrum composed of a soft, thermal component joined by a hard powerlaw tail that dominates the spectrum above $\sim 2-3$ keV (Degenaar et al. 2009, see also Sections 2.1 and 2.2). This is frequently seen for neutron star X-ray binaries in quiescence (e.g., Rutledge et al. 1999; in't Zand et al. 2001; Tomsick et al. 2004). The non-thermal component is usually well-fitted by a simple powerlaw with index 1–2 (e.g., Asai et al. 1996). The fractional contribution of the hard powerlaw tail to the 0.5–10 keV X-ray flux widely varies amongst sources and possibly also with changing luminosity (Jonker et al. 2004; Jonker 2008). The physical process that yields the powerlaw spectral component remains elusive (see e.g., Campana et al. 1998; Campana 2003).

Although the soft spectral component has been ascribed to low-level accretion onto the neutron star (Zampieri et al. 1995), it is most often interpreted as thermal surface radiation resulting from deep crustal heating (Brown et al. 1998). According to this model, the accretion of matter compresses the neutron star crust, which induces a series of reactions that deposit heat (e.g., Haensel & Zdunik 1990, 2003, 2008; Gupta et al. 2007). The heat energy gained via this process is subsequently lost during quiescent episodes, resulting in a candescent thermal emission from the neutron star surface set by the time-averaged accretion rate of the system, as well as the rate of neutrino emissions from the stellar core (e.g., Brown et al. 1998; Colpi et al. 2001). The latter cools the interior and depends on the equation of state of cold nuclear matter and the central density of the neutron star (e.g., Yakovlev et al. 2003; Yakovlev & Pethick 2004). Observations of quiescent neutron stars can thus provide insight into their interior properties.

In this context, a special opportunity arises for the quasi-persistent neutron star X-ray binaries. In 2001, both KS 1731–260 and MXB 1659–29 made the transition to quiescence, following accretion episodes of 12.5 and 2.5 years, respectively (Wijnands et al. 2001, 2002, 2003, 2004; Cackett et al. 2006, 2008). More recently, in 2007, the $\sim$ 1.6-year long outburst of XTE J1701–462 came to a halt (Altamirano et al. 2007; Homan et al. 2007; Fridriksson et al. 2010). All three systems were subsequently monitored with *Chandra* and *XMM-Newton*, which revealed that thermal flux and neutron star temperature were gradually decreasing over the course of years (see also Section 4). This can be interpreted as cooling of the neutron star crust that has been heated during the prolonged accretion outburst (Wijnands et al. 2001; Rutledge et al. 2002). Successful modelling of the observed quiescent X-ray lightcurves with neutron star thermal evolution models supports this hypothesis and provides important constraints on the crust properties, such as the thermal conductivity (Shternin et al. 2007; Brown & Cumming 2009).

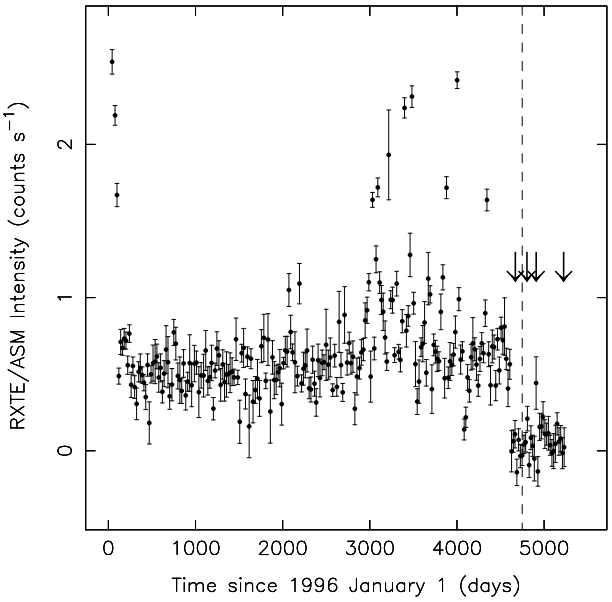

Figure 1. *RXTE*/ASM 20-day averaged lightcurve (1.5–12 keV) of EXO 0748–676, illustrating the cessation of the outburst in late 2008. The dashed vertical line corresponds to 2008 December 31. The arrows indicate the times of our four sequences of *Chandra* observations, which were performed when the source dropped below the detection limit of *RXTE* (both of the ASM and the PCA).

Along these lines we have pursued an observational campaign of EXO 0748–676 to study the time evolution of the quiescent X-ray emission following its long accretion outburst. In Degenaar et al. (2009), we reported on *Chandra* and *Swift* observations obtained between 2008 September 28 and 2009 January 30. We found a relatively hot and luminous quiescent system with a temperature of $kT_{\rm eff}^{\infty} \sim 0.11-0.13$ keV and a thermal 0.01–100 keV luminosity of $\sim (8-16)\times10^{33}$ (d/7.4 kpc)^2 erg s^{-1}. No clear decrease in effective temperature and thermal bolometric flux was found over the five-month time span.

In this paper we report on continued *Swift* and *Chandra* observations of EXO 0748–676 during its quiescent state. In addition we include an archival *XMM-Newton* observation performed $\sim$ 2 months after the cessation of the outburst. Previous *Chandra* and *Swift* observations discussed by Degenaar et al. (2009) were re-analysed in this paper in order to obtain a homogenous quiescent lightcurve.

2 OBSERVATIONS AND DATA ANALYSIS

Table 1 gives an overview of all new observations of EXO 0748–676 discussed in this paper. A list of earlier *Chan-*

Table 1. Observation log.

Satellite	Obs ID	Date	Exp. time (ks)
XMM	0560180701*	2008-11-06	29.0 (MOS) 22.9 (PN)
Swift	31272016	2009-02-13	3.5
Swift	31272017	2009-02-20	4.1
Swift	31272018*	2009-02-23	5.1
Chandra	9071*	2009-02-23/24	15.8
	10871*	2009-02-25	9.6
Swift	31272019*	2009-03-01	3.2
Swift	31272020	2009-03-10	5.1
Swift	31272021	2009-03-16	4.6
Swift	31272022	2009-04-09	3.5
Swift	31272023	2009-04-16	2.8
Swift	31272024	2009-04-23	4.8
Swift	31272025	2009-05-07	4.5
Swift	31272026	2009-05-14	3.6
Swift	31272027	2009-05-28	3.4
Swift	31272028	2009-06-05	4.1
Chandra	9072*	2009-06-10	27.2
Swift	31272029*	2009-06-11	4.3
Swift	31272030	2009-06-18	3.9
Swift	31272031*	2009-06-26	5.5
Swift	31272032*	2009-07-03	4.8
Swift	31272033	2009-07-18	5.5
Swift	31272034*	2009-07-25	5.8
Swift	31272035*	2009-07-31	10.3
Swift	31272036*	2009-08-15	9.4
Swift	31272037	2009-08-25	1.1
Swift	31272038	2009-08-26	7.4
Swift	31272039*	2009-09-08	4.7
Swift	31272040*	2009-09-09	4.3
Swift	31272041	2009-10-01	1.9
Swift	31272042	2009-10-02	1.8
Swift	31272043	2009-10-07	2.0
Swift	31272044	2009-10-08	2.4
Swift	31272045	2009-10-09	2.3
Swift	31272046*	2009-11-05	4.2
Swift	31272047*	2009-12-21	9.4
Swift	31272048*	2010-10-01	9.6
Swift	31272049	2010-02-12/13	11.3
Swift	31272050*	2010-03-12/13	9.5
Chandra	11059*	2010-04-20	27.4

Note. – The observations marked with an asterisk contain (part of) eclipses. The listed exposure times represent the duration of the observations uncorrected for eclipses.

dra and *Swift* observations in quiescence can be found in Degenaar et al. (2009).

2.1 *XMM-Newton*

EXO 0748–676 was observed with the European Photon Imaging Camera (EPIC) onboard *XMM-Newton* on 2008 November 6 from 08:30–16:42 UT (see also Bassa et al. 2009). Both the MOS detectors and the PN camera were operated in full window mode and using the medium optical blocking filter. Data reduction and analysis was carried out with the Science Analysis Software (SAS; v. 9.0.0). We reprocessed the Original Data Files (ODF) using the tasks EMPROC and EPPROC. To identify possible periods of high particle background, we extracted high-energy lightcurves ($\geqslant$ 10 keV for the MOS and between 10–12 keV for the PN). No strong background flares occurred during the observation. The net exposure times are 29.0 and 22.9 ks for the MOS and PN, respectively. EXO 0748–676 is detected at count rates of 0.16 ± 0.01 counts s^{-1} (MOS) and 0.55 ± 0.01 counts s^{-1} (PN).

Source spectra and lightcurves were obtained with the software task EVSELECT, using a 35 arcsec circular region and applying pattern selections 0–12 and 0–4 for the MOS and PN data, respectively. Corresponding background events were extracted from a circular region with a radius 70 arcsec. For the MOS cameras, the background was positioned on a source-free region on the same CCD as the source. For the PN instrument the background events were extracted from an adjacent CCD, at the same distance from the readout node to ensure similar low-energy noise. The ancillary response files (arf) and redistribution matrices (rmf) were generated with the tasks ARFGEN and RMFGEN.

The EPIC lightcurves show two full eclipses (see also Bassa et al. 2009), corresponding to eclipse cycles 54384 and 54385 in the numbering system of Parmar et al. (1986). To calculate the correct non-eclipse time-averaged fluxes, we reduce the exposure times for each instrument by 500 s per eclipse, which is the approximate length of the eclipses of EXO 0748–676 (Parmar et al. 1986; Wolff et al. 2009). Using the tool GRPPHA, the spectra were grouped to contain a minimum of 20 photons per bin. The combined MOS and PN spectral data were fitted in XSPEC (v. 12) in the 0.5–10 keV energy range, with all spectral parameters tied between the three EPIC detectors.

A single absorbed powerlaw model provides an acceptable fit to the *XMM-Newton* data (red. $\chi^2 = 1.3$ for 466 d.o.f.). However, the spectral index is unusually large for an X-ray binary ($\Gamma = 4.7 \pm 0.1$) and suggests that the spectrum has a thermal shape. A simple absorbed blackbody model, BBODYRAD, provides an adequate fit ($\chi^2 = 1.2$ for 466 d.o.f.), although the inferred emitting region has a much smaller radius than expected for a neutron star ($\sim 2-4$ km for distances of $5-10$ kpc). However, it is thought that radiative transfer effects in the neutron star atmosphere cause the emergent spectrum to deviate from a blackbody (e.g., Zavlin et al. 1996; Rutledge et al. 1999). There are several neutron star atmosphere models available within XSPEC, which yield equivalent results (see e.g., Heinke et al. 2006; Webb & Barret 2007). In the remainder of this work, we concentrate on fitting the data with a neutron star atmosphere model NSATMOS (Heinke et al. 2006).

The model parameters are the hydrogen column density ($N_{\rm H}$), the neutron star mass and radius ($M_{\rm NS}$ and $R_{\rm NS}$), the effective temperature in the neutron star frame (i.e., non-redshifted; $kT_{\rm eff}$), the source distance (D) and a normalisation factor, which parametrizes the fraction of the surface that is radiating. We keep the latter fixed at 1 throughout this work, which corresponds to the entire neutron star surface emitting. The effective temperature as seen by an observer at infinity is given by $kT_{\rm eff}^{\infty} = kT_{\rm eff} \times g_r$, where $g_r = \sqrt{1-(2GM_{\rm NS})/(R_{\rm NS}c^2)}$ is the gravitational redshift, G the gravitational constant and c the speed of light.

The NSATMOS model provides a good fit to the data ($\chi^2 = 1.1$ for 466 d.o.f.), although significant residuals above the model fit are present for energies $\gtrsim 2-3$ keV. We model this non-thermal emission by adding a powerlaw compo-

nent, which significantly improves the fit ($\chi^2 = 1.0$ for 464 d.o.f.; an F-test suggests a $\sim 1 \times 10^{-14}$ probability of achieving this level of improvement by chance). *Chandra* observations carried out in 2008 mid-October, three weeks prior to this *XMM-Newton* observation, also indicated the presence of a non-thermal component in the quiescent spectrum of EXO 0748–676 (Degenaar et al. 2009). Whereas the *Chandra* data could not constrain the powerlaw index, the larger collective area of *XMM-Newton* provides better constraints for the fluxes under consideration.

By fitting the *XMM-Newton* data to a combined NSATMOS and powerlaw model, we obtain a powerlaw index of $\Gamma = 1.7 \pm 0.5$, i.e., in between the values of $\Gamma = 1$ and $\Gamma = 2$ considered by Degenaar et al. (2009). For this fit, which furthermore yields $N_{\rm H} = (7 \pm 2) \times 10^{20}$ cm^{-2} and $R_{\rm NS} = 17.8 \pm 1$ km for fixed values of $D = 7.4$ kpc and $M_{\rm NS} = 1.4$ M$_\odot$, the powerlaw component contributes ~ 10 percent to the total unabsorbed 0.5–10 keV flux. This is lower than the $\sim 15 - 20$ percent inferred from the *Chandra* observations performed in 2008 mid-October (Degenaar et al. 2009). The obtained hydrogen column density is consistent with values found for EXO 0748–676 during its outburst ($N_{\rm H} \sim (7 - 12) \times 10^{20}$ cm^{-2}, e.g., Sidoli et al. 2005).

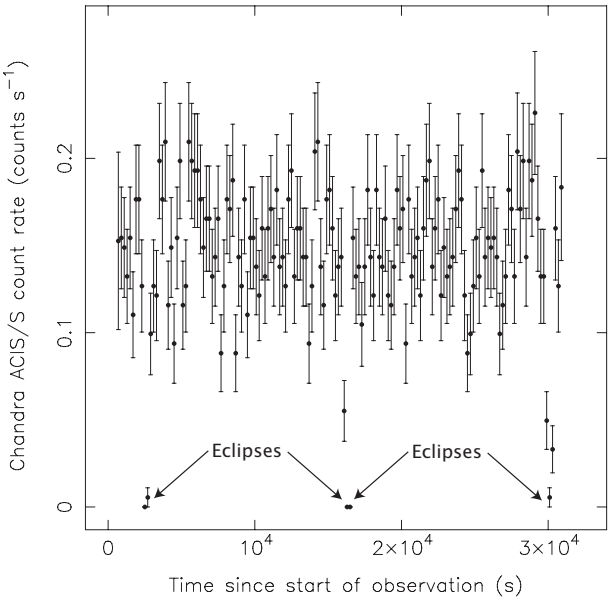

Figure 2. *Chandra*/ACIS-S 0.5–8 keV lightcurve of EXO 0748–676 obtained on 2010 April 20 (obs ID 11059). Each point represents 200 s of data. Three eclipses are visible.

2.2 *Chandra*

We obtained three new *Chandra*/ACIS-S observations. The first consists of two separate exposures obtained on 2009 February 23–24 22:07–03:15 UT (obs ID 9071) and 2009 February 25 12:32–15:59 UT (obs ID 10871), lasting for ~ 15.8 and ~ 9.6 ks, respectively. In both data sets, EXO 0748–676 is clearly detected at a count rate of 0.17 ± 0.01 counts s^{-1} (0.5–8 keV). This is a factor ~ 1.5 lower than observed in 2008 October, when the source was detected with *Chandra*/ACIS-S at a rate of 0.24 ± 0.01 counts s^{-1}. Two full eclipses are seen in the lightcurve of observation 9071, while one eclipse is present in that of 10871 (eclipse cycle numbers 55071, 55072 and 55080, respectively).

A second *Chandra* observation was carried out on 2009 June 10, from 12:36–21:16 UT, with an exposure time of 27.2 ks (obs ID 9072). In this observation EXO 0748–676 is detected at a count rate of 0.16 ± 0.01 counts s^{-1} and the lightcurve shows two full eclipses (cycles 55740 and 55741). Furthermore, a 27.4 ks exposure was taken on 2010 April 20 from 02:37–11:28 UT (obs ID 11059), which captured three full eclipses (see Fig. 2, these correspond to eclipse cycle numbers 57708, 57709 and 57710), and detected the source at a count rate of 0.14 ± 0.01 counts s^{-1}. Similar to our treatment of the *XMM-Newton* data, we reduce the exposure times of all *Chandra* observations by 500 s per eclipse. There are no indications of background flares, so the full data set is used in further analysis.

We reduced the data employing the CIAO tools (v. 4.2) and standard *Chandra* analysis threads. For all three observation sequences, the ACIS-S3 CCD was operated in a 1/8 sub-array, resulting in a frame-time of 0.4 s. For the observed count rates, the pile-up fraction is < 2 percent, so no further corrections were made. Spectra were extracted with the tool PSEXTRACT, while the rmf and arf files were created using MKACISRMF and MKARF, respectively. We employ a circular region of 3 arcsec to obtain source events and a 10–25 arcsec annulus for the background. We also reprocessed the *Chandra* observation obtained in 2008 October (see Degenaar et al. 2009) to benefit from the calibration update that was released in 2009 December. Prior to spectral fitting, the spectra were grouped to contain at least 20 photons per bin. We find no spectral differences between the two separate exposures performed in 2009 February and therefore we tie all parameters for these two spectra in the main fits.

The *Chandra* observations obtained in 2009 February and June are well-fitted by a single-component thermal model, but the 2010 April data shows significant residuals at energies $\gtrsim 2 - 3$ keV. If we include a powerlaw with photon index $\Gamma = 1.7$, as found from fitting the *XMM-Newton* data (see Section 2.1), this model component contributes ~ 10, ~ 5 and ~ 15 percent to the total unabsorbed 0.5–10 keV flux for the data taken in 2009 February, June and 2010 April, respectively. Fig. 3 compares the *Chandra* spectral data obtained on 2008 October and 2010 April, showing that both spectral components decreased over the 18-month time span that separates the two observations.

2.3 *Swift*

In addition to the *Chandra* and *XMM-Newton* observations, we have been monitoring EXO 0748–676 on a regular basis with the XRT aboard the *Swift* satellite. Starting in 2008 late-September, approximately $2 - 3$ pointings were performed each month with a typical duration of $\sim 3 - 5$ ks per observation, and a separation of $\sim 1 - 2$ weeks. From 2009 November onwards, the cadence was lowered to one observation per month with a longer exposure time when possible (see Table 1). EXO 0748–676 is detected in the XRT observations at count rates of $\sim (1 - 5) \times 10^{-2}$ counts s^{-1}.

All *Swift*/XRT observations were obtained in the photon-counting (pc) mode and were processed using the

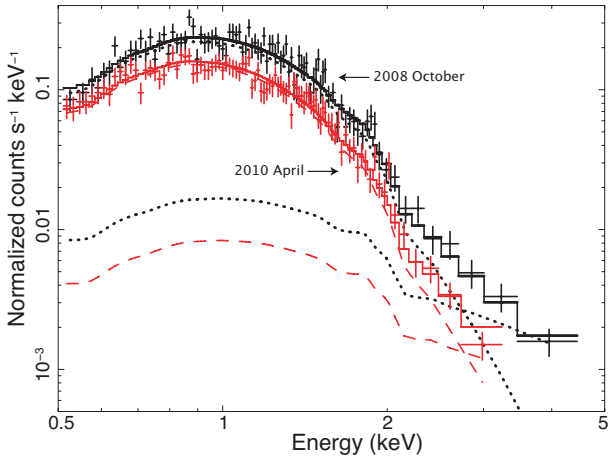

Figure 3. Spectra of the *Chandra* observations of 2008 October (black) and 2010 April (red), along with the model fits (solid lines). The dotted and dashed lines represent the contributions of the NSATMOS and powerlaw components for the 2008 and 2010 data, respectively.

XRTPIPELINE with standard quality cuts (event grade 0–12). Using XSELECT (v. 2.4), we extracted source spectra from a circular region with a radius of 35 arcsec ($\sim$ 15 pixels), which optimises the signal to noise ratio at the observed count rates (Evans et al. 2007). Corresponding background events were averaged over three source-free regions of similar shape and size. Employing the tool XRTEXPOMAP, we created exposure maps to account for the effective area of the CDD, while arfs generated with XRTMKARF account for vignetting and point-spread-function corrections. The latest rmf (v. 11) was obtained from the CALDB database.

We reduced the exposure times of those observations that contained eclipses according to the ephemeris of Wolff et al. (2009) to calculate the correct non-eclipse time-averaged fluxes (see Table 1). Furthermore, *Swift* observations obtained within a 2-day time span were summed to improve the data statistics[1]. This seems justified, since the *Chandra* data do not reveal any spectral changes on such time scales (see Section 2.2).

3 RESULTS

3.1 Spectral fits

We first fit the *Chandra* and *XMM-Newton* data simultaneously to an absorbed NSATMOS model joined by a powerlaw, to explore the best-fit values for the neutron star mass and radius, source distance and hydrogen column density. We include the first set of *Chandra* observations obtained in 2008 October (discussed in Degenaar et al. 2009) in the analysis. For the neutral hydrogen absorption, we use the PHABS model with the default XSPEC abundances and cross-sections. The powerlaw index is fixed to $\Gamma = 1.7$ (the best fit-value obtained from *XMM-Newton* observations; see Section 2.1), because there are not sufficient counts at higher energies in either the *Swift* or the *Chandra* spectra to allow this component to vary. The powerlaw normalisation is left as a free parameter.

If the neutron star mass and radius are fixed to canonical values of $M_{\rm NS} = 1.4$ M$_\odot$ and $R = 10$ km, and in addition the source distance is fixed to the best estimate obtained from type-I X-ray bursts ($D = 7.4$ kpc; Galloway et al. 2008), the hydrogen column density pegs at its lower limit ($N_{\rm H} = 0$). When the distance is left to vary freely, the best-fit value is 4.6 ± 0.3 kpc, which is just outside the range obtained from X-ray burst analysis (5–8.3 kpc; Galloway et al. 2008). Therefore, we choose to keep the distance fixed at 7.4 kpc, and instead allow the neutron star radius to vary. This way, we obtain best-fit values of $N_{\rm H} = (7\pm1)\times10^{20}$ cm^{-2} and $R = 15.6\pm0.8$ km. If additionally the neutron star mass is left free to vary in the fit, this parameter is not strongly constrained ($M_{\rm NS} \sim 1.6\pm0.6$ M$_\odot$). In the final fits we choose to fix the neutron star mass to $M_{\rm NS} = 1.4$ M$_\odot$, because otherwise the uncertainty in this quantity will dominate the errors of the other parameters.

The *Swift* data do not provide sufficient statistics to constrain the powerlaw component. We do include a powerlaw in the fits, but fix both the index and the normalisation of this component. Since it is unclear how the powerlaw exactly evolves over time, we adjust the powerlaw normalisation for the *Swift* observations such that it always contributes 10 percent of the total unabsorbed 0.5–10 keV flux. After treating each *Swift* observation separately, we found that the thermal flux and neutron star temperature did not evolve significantly between consecutive observations. To improve the statistics, we therefore sum the *Swift* data into groups spanning $\sim 1-4$ weeks of observations, resulting in exposure times of $\sim 10-20$ ks (see Table 2). These spectra were grouped to contain a minimum of 20 photons per bin.

For the final spectral analysis, we fit all *XMM-Newton*, *Chandra* and *Swift* data with an absorbed NSATMOS plus powerlaw model, where $N_{\rm H} = 7\times10^{20}$ cm^{-2}, $M_{\rm NS} = 1.4$ M$_\odot$, $R_{\rm NS} = 15.6$ km, $D = 7.4$ kpc and $\Gamma = 1.7$ are fixed, while the neutron star effective temperature is left as a free parameter. The powerlaw normalisation is fixed for the *Swift* data, but left to vary freely for the *Chandra* and *XMM-Newton* observations. We fit all data in the 0.5–10 keV energy range and deduce the absorbed and unabsorbed fluxes in this band. The thermal model fit is extrapolated to the energy range of 0.01–100 keV to estimate the thermal bolometric flux. The results from fitting the X-ray spectra in this way are presented in Table 2. The effective temperatures and thermal bolometric fluxes derived from *Chandra*, *Swift* and *XMM-Newton* data are displayed in Fig. 4. Examination of Fig. 4 suggests that there is a small but discernible offset in the thermal flux and neutron star temperature as deduced from the different satellites. This is briefly discussed in Section 3.3.

3.2 Lightcurve fits

Fig. 4 clearly reveals a decaying trend in thermal flux and temperature. To investigate the decay shape, we fit the temperature curve with an exponential decay function of the form $y(t) = a\ e^{-(t-t_0)/\tau}$, where a is a normalisation constant, t_0 is the start time of the cooling curve and τ the e-folding time. Given the offset between the different in-

[1] This is the case for obs IDs 31272037/38, 31272039/40 and 31272043/44/45; see Table 1.

Table 2. Results from fitting the spectral data.

Satellite	Date	Δt (days)	Pow. frac. (%)	$kT_{\rm eff}^{\infty}$ (eV)	$F_{\rm X}$	$F_{\rm bol}^{\rm th}$	$L_{\rm bol}$	Red. χ^2 (d.o.f.)
Swift†	2008-09-28 – 2008-10-07	4.9	10 fix	123.7 ± 5.4	1.31 ± 0.22	1.53 ± 0.26	10.0 ± 1.7	0.93 (8)
Chandra†	2008-10-12/13/15	1.4	20 ± 3	118.8 ± 0.9	1.23 ± 0.02	1.31 ± 0.04	8.6 ± 0.3	1.03 (175)
Swift†	2008-10-29 – 2008-11-02	2.2	10 fix	118.3 ± 2.6	1.10 ± 0.09	1.28 ± 0.11	8.4 ± 0.7	0.67 (14)
XMM	2008-11-06	0.2	7 ± 2	120.7 ± 0.4	1.14 ± 0.01	1.39 ± 0.02	9.1 ± 0.1	1.08 (467)
Swift†	2008-11-28 – 2008-12-20	11.0	10 fix	118.7 ± 2.6	1.11 ± 0.10	1.30 ± 0.12	8.5 ± 0.8	1.09 (14)
Swift†	2009-01-10 – 2009-01-30	9.8	10 fix	116.2 ± 2.2	0.99 ± 0.07	1.19 ± 0.09	7.8 ± 0.6	1.09 (18)
Swift	2009-02-13 – 2009-02-23	5.1	10 fix	117.2 ± 2.4	1.02 ± 0.08	1.23 ± 0.10	8.1 ± 0.7	0.50 (15)
Chandra	2009-02-23/25	0.9	12 ± 4	113.5 ± 1.3	0.91 ± 0.03	1.09 ± 0.05	7.1 ± 0.3	0.90 (139)
Swift	2009-03-01 – 2009-03-16	7.2	10 fix	115.6 ± 2.3	0.97 ± 0.08	1.17 ± 0.09	7.7 ± 0.6	0.79 (16)
Swift	2009-04-09 – 2009-04-23	7.1	10 fix	112.2 ± 2.8	0.86 ± 0.09	1.03 ± 0.11	6.8 ± 0.7	1.16 (10)
Swift	2009-05-07 – 2009-06-05	14.7	10 fix	114.2 ± 2.3	0.92 ± 0.07	1.11 ± 0.09	7.3 ± 0.6	0.88 (16)
Chandra	2009-06-10	0.2	4 ± 3	111.0 ± 0.7	0.75 ± 0.01	0.99 ± 0.03	6.5 ± 0.2	1.19 (93)
Swift	2009-06-11 – 2009-07-03	11.5	10 fix	111.9 ± 2.2	0.75 ± 0.07	1.03 ± 0.08	6.7 ± 0.5	0.99 (17)
Swift	2009-07-18 – 2009-07-31	6.9	10 fix	110.5 ± 2.1	0.79 ± 0.06	0.98 ± 0.07	6.4 ± 0.5	0.42 (18)
Swift	2009-08-15 – 2009-09-09	12.7	10 fix	110.0 ± 1.8	0.78 ± 0.05	0.96 ± 0.06	6.3 ± 0.4	1.30 (26)
Swift	2009-10-01 – 2009-11-05	17.4	10 fix	108.0 ± 2.6	0.69 ± 0.07	0.88 ± 0.09	5.8 ± 0.6	1.49 (11)
Swift	2009-12-21 – 2010-10-01	10.2	10 fix	109.4 ± 2.0	0.74 ± 0.06	0.94 ± 0.07	6.1 ± 0.5	1.51 (19)
Swift	2010-02-12 – 2010-03-13	15.0	10 fix	109.4 ± 2.0	0.76 ± 0.06	0.94 ± 0.07	6.1 ± 0.5	1.25 (20)
Chandra	2010-04-20	0.2	15 ± 4	108.6 ± 1.1	0.77 ± 0.02	0.91 ± 0.04	6.0 ± 0.2	0.79 (91)

Note. – The observations marked by a dagger were already discussed in Degenaar et al. (2009), but re-fitted in this work. These results were obtained by using a combined absorbed `NSATMOS` and powerlaw model, where $N_{\rm H} = 7 \times 10^{20}$ cm^{-2}, $M_{\rm NS} = 1.4$ M$_{\odot}$, $R_{\rm NS} = 15.6$ km, $D = 7.4$ kpc and $\Gamma = 1.7$ were kept fixed. The quoted errors represent 90% confidence levels. $F_{\rm X}$ represents the 0.5–10 keV total model flux and $F_{\rm bol}^{\rm th}$ gives the 0.01–100 keV `NSATMOS` flux; both are unabsorbed and in units of 10^{-12} erg cm^{-2} s^{-1}. $L_{\rm bol}$ gives the 0.01–100 keV luminosity of the `NSATMOS` model component in units of 10^{33} erg s^{-1} and assuming a source distance of D=7.4 kpc. Δt represents the time interval of the observations in days and the fractional powerlaw contribution is given in a percentage of the total unabsorbed 0.5–10 keV flux.

struments (see Section 3.3), we perform different fits to the *Chandra* and *Swift* data. We fix t_0 to 2009 September 5 (MJD 54714), which is in between the first non-detection by *RXTE*/PCA and the first *Swift* observation of the source (see Degenaar et al. 2009).

This simple exponential decay, represented by the dotted lines in Fig. 5, yields an e-folding time of 6121.7 ± 2004.0 days for the *Chandra* data, but does not provide a good fit (red. $\chi^2 = 6.0$ for 2 d.o.f.). For the *Swift* lightcurve we find $\tau = 5328.1 \pm 674.7$ days (red. $\chi^2 = 0.5$ for 12 d.o.f.). If we include a constant offset (i.e., $y(t) = a\ e^{-(t-t_0)/\tau} + b$), we obtain a better fit for the *Chandra* data (solid lines in Fig. 5), yielding a normalisation of 13.4 ± 0.2 eV, an e-folding decay time of 191.6 ± 9.7 days and a constant level of 107.9 ± 0.2 eV (red. $\chi^2 = 0.02$ for 1 d.o.f.). For the *Swift* data this results in $a = 17.2 \pm 1.8$ eV, $\tau = 265.6 \pm 100.0$ days and $b = 106.2 \pm 2.5$ eV (red. $\chi^2 = 0.34$ for 11 d.o.f.), which is consistent with the *Chandra* fit.

Although an exponential decay provides an adequate description of the data of EXO 0748–676, as has been found for other sources (e.g., Cackett et al. 2006; Fridriksson et al. 2010), mathematically a neutron star crust is expected to cool via a (broken) powerlaw (Eichler & Cheng 1989; Brown & Cumming 2009). If we fit a single powerlaw of the form $y(t) = A(t-t_0)^B$ to the *Chandra* data, we find an index of -0.03 ± 0.01 and a normalisation of 134.4 ± 1.0 eV (red. $\chi^2 = 0.13$ for 2 d.o.f.). For the *Swift* observations we find $B = -0.05 \pm 0.01$ and $A = 144.7 \pm 3.8$ eV (red. $\chi^2 = 0.4$ for 12 d.o.f.). These powerlaw fits are indicated by the dashed lines in Fig. 5.

A broken powerlaw also yields an acceptable fit to the *Swift* data (red. $\chi^2 = 0.3$ for 10 d.o.f.). We find a normalisation of $A = 135.0 \pm 17.8$ eV, a break at 166.0 ± 99.2 days and decay indices of -0.03 ± 0.03 and -0.06 ± 0.02 before and after the break, respectively. This fit is indicated by the dashed-dotted curve in Fig. 5. There are not sufficient *Chandra* observations to fit a broken powerlaw decay. We note that the shape of the decay curve of EXO 0748–676 is not strongly affected by our choice of spectral parameters ($N_{\rm H}$, $M_{\rm NS}$, $R_{\rm NS}$, and Γ) or assumed distance (see also previous studies by e.g., Wijnands et al. 2004; Cackett et al. 2008).

3.3 Instrument cross-calibration

The quiescent lightcurve presented in Fig. 4 indicates that the thermal flux and temperature inferred from the *XMM-Newton* observation lie exactly on the trend indicated by the *Swift* data points. However, the *Chandra* results are systematically lower. This apparent offset (~ 6 percent for the flux lightcurve) is possibly due to cross-calibration issues between the two satellites (see e.g., Kirsch et al. 2005). Such a discrepancy has not been found for *Swift* and *XMM-Newton* (e.g., Kirsch et al. 2005), which appears to be reflected in our results as well. We note that regardless of the offset between the *Chandra* and *Swift* points, both data sets show a similar decay in thermal flux and neutron star temperature (see Section 3.2).

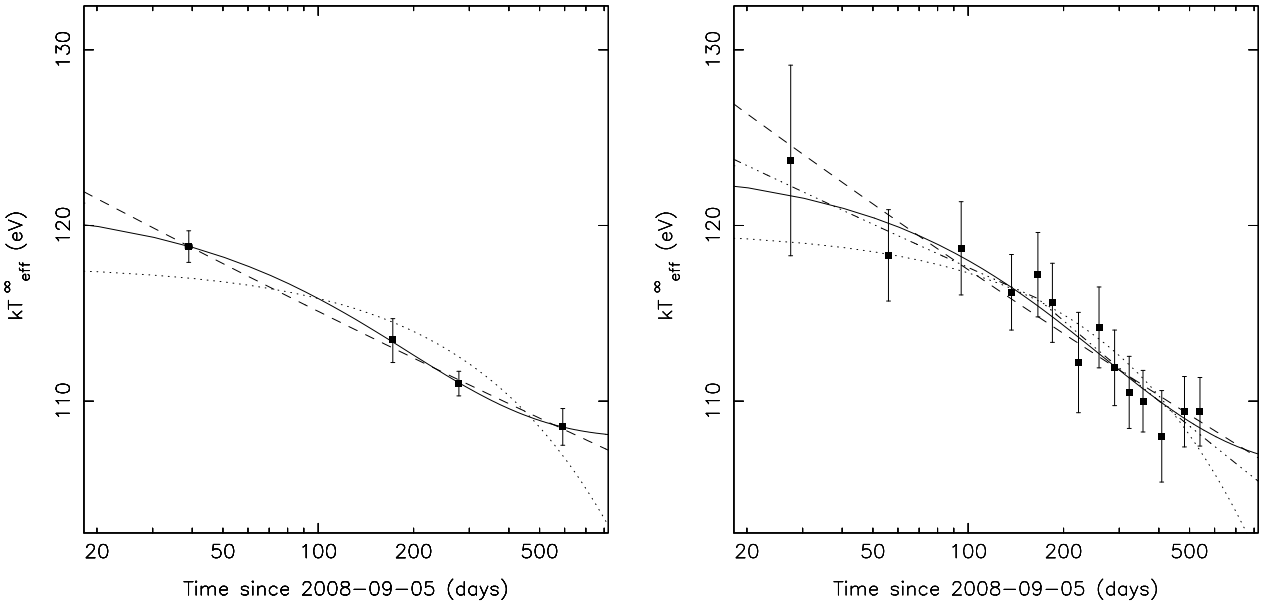

Figure 5. Evolution of the effective temperature of EXO 0748–676 fitted to different decay functions (see Section 3.2). The left image displays *Chandra* data and exponential decay fits both with and without a constant offset (solid and dotted line, respectively), as well as a decaying powerlaw (dashed curve). The right image shows *Swift* observations, where the dashed line is again a powerlaw fit, while the solid and dotted curves are exponential decays. In addition, this plot includes a fit to a broken powerlaw, which is represented by the dashed-dotted line.

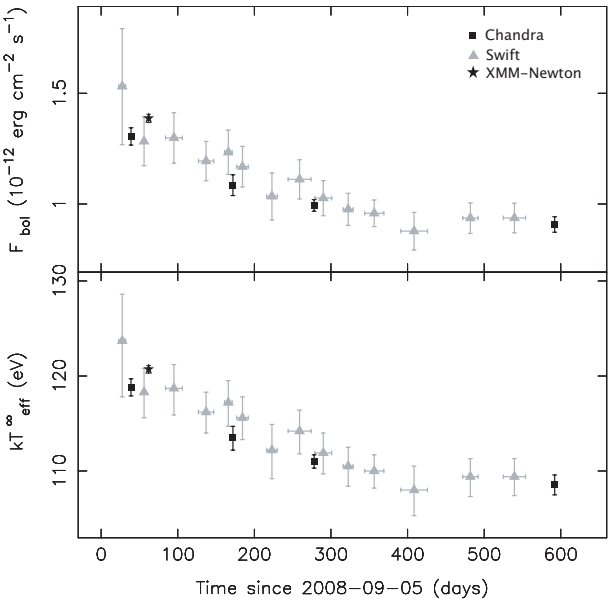

Figure 4. Evolution of the bolometric flux (top) and effective temperature (bottom) of EXO 0748–676, deduced from *Chandra*/ACIS-S (black squares), *Swift*/XRT (grey triangles) and *XMM-Newton*/EPIC (black star) data. Multiple *Swift* observations were summed to improve the data statistics (see Section 2.3).

4 DISCUSSION

We discuss *Chandra*, *Swift* and *XMM-Newton* observations obtained after the cessation of the very long (∼24 year) active period of EXO 0748–676. The data cover the first 19 months (1.6 years) of the quiescent phase. By assuming a neutron star atmosphere model NSATMOS, we find a clear decrease in neutron star effective temperature from $kT_{\rm eff}^{\infty} \sim 124$ to 109 eV. The thermal bolometric flux decayed from $F_{\rm bol}^{\rm th} \sim 1.5 \times 10^{-12}$ to 0.9×10^{-12} erg cm^{-2} s^{-1}.

In addition to a soft, thermal component, the *Chandra* and *XMM-Newton* observations show evidence for a hard powerlaw tail with index $\Gamma = 1.7$. The fractional contribution of the hard spectral component to the total unabsorbed 0.5–10 keV flux initially decreased from ∼ 20 percent in 2008 October to ∼ 4 percent in 2009 June. However observations carried out in 2010 April suggest that the powerlaw fraction increased again to ∼ 15 percent. Similar behavior has been observed for several other quiescent neutron star systems (Jonker et al. 2004; Jonker 2008), although others show more irregular behaviour (Fridriksson et al. 2010). In Cen X-4, the powerlaw tail in the quiescent spectrum shows variations that appear to be linked to changes in the thermal component, possibly caused by low-level accretion (Cackett et al. 2010).

The gradual decrease in thermal flux and neutron star temperature observed for EXO 0748–676 can be interpreted as the neutron star crust cooling down in quiescence after it has been heated during its long accretion outburst. Fig. 6 compares our data of EXO 0748–676 with the crust cooling curves observed for the neutron star X-ray binaries KS 1731–260, MXB 1659–29 and XTE J1701–462. This plot clearly shows that the quiescent lightcurve of EXO 0748–676 is relatively flat compared to the others. We have observed our target over the first ∼ 19 months after the cessation of the outburst and during this time the thermal bolometric flux has decreased by a factor of ∼ 1.7. In a similar time span, the thermal bolometric fluxes of KS 1731–260, MXB 1659–29 and XTE J1701–462 had decreased by a factor of ∼ 3.5, 6 and 2.5, respectively (see Cackett et al. 2006;

Fridriksson et al. 2010). The effective neutron star temperature of EXO 0748–676 has decreased by about 10%, compared to ~ 30, 40 and 20% for KS 1731–260, MXB 1659–29 and XTE J1701–462.

Although the observed fractional changes in neutron star temperature and thermal bolometric flux are smaller for EXO 0748–676 than for the other three sources, the decay itself may not be markedly different. The quiescent lightcurves of KS 1731–260, MXB 1659–29 and XTE J1701–462 can be fit with an exponential decay function levelling off to a constant value, yielding e-folding times of $\sim 305 \pm 50$, $\sim 465 \pm 25$ and $\sim 120 \pm 25$ days, respectively (Cackett et al. 2008; Fridriksson et al. 2010). For the *Chandra* data of EXO 0748–676, we find an e-folding time of $\sim 192 \pm 10$ days (see Section 3.2). These decay times provide a measure of the thermal relaxation time of the neutron star crust, which depends on the composition and structure of the lattice, the distribution of heating sources and the thickness of the crust (e.g., Lattimer et al. 1994; Rutledge et al. 2002; Shternin et al. 2007; Brown & Cumming 2009).

Rutledge et al. (2002) and Shternin et al. (2007) calculate theoretical cooling curves for KS 1731–260, assuming different physics for the crust and core. These authors present simulations for both an amorphous crust and an ordered crystalline lattice. For the latter, the spread of nuclide charge numbers (Z) in the crust matter is small, which is referred to as a low level of impurities, and results in a highly conductive crust. A large number of impurities gives an amorphous structure, which affects the thermal properties of the crust and results in a low conductivity. In addition, Rutledge et al. (2002) explore standard (i.e., slow) and enhanced neutrino cooling mechanisms, yielding different core temperatures. Comparing our results on EXO 0748–676 with the decay shapes resulting from those calculations suggests that the neutron star has a highly conductive crust, similar to what has been inferred for the other three sources (Wijnands et al. 2002, 2004; Cackett et al. 2006; Shternin et al. 2007; Brown & Cumming 2009; Fridriksson et al. 2010). The fact that the decay curve of EXO 0748–676 is rather flat may be explained in terms of a relatively small temperature gradient and thus lower thermal flux across the core-crust boundary (compare the model curves of Rutledge et al. 2002, for a highly conductive crust and different core temperatures). This can be due to a combination of a warm neutron star core (see below) and a relatively low mass-accretion rate during outburst.

The exponential decay fit to the *Chandra* data of EXO 0748–676 indicates that the neutron star crust might already be close to restoring equllibrium with the core. The fit results in a quiescent base level of 107.9 ± 0.2 eV, while we found a temperature of 108.6 ± 1.1 eV for the observation performed in 2010 April. Prior to its last outburst, EXO 0748–676 was observed in quiescence with the *EINSTEIN* observatory, displaying a 0.5–10 keV unabsorbed flux of $(8.4^{+4.2}_{-1.7}) \times 10^{-13}$ erg cm^{-2} s^{-1} (Garcia & Callanan 1999). Our *Chandra* observations of 2010 April detected EXO 0748–676 at a 0.5–10 keV unabsorbed flux of $(7.7 \pm 0.2) \times 10^{-13}$ erg cm^{-2} s^{-1} (see Table 2). Assuming that the *EINSTEIN* detection caught EXO 0748–676 at its quiescent base level, this supports the idea that the crust has nearly cooled down. This would imply that the neutron star in EXO 0748–676 is relatively hot (cf. Heinke et al. 2009), suggesting that either standard cooling mechanisms are operating in the core and that the neutron star is not very massive, or that the time-averaged mass-accretion rate of the system is very high.

The nuclear reactions induced in the crust of an accreting neutron star are expected to generate a thermal luminosity of $L_{\rm bol} \sim \langle \dot{M} \rangle Q_{\rm nuc}/m_{\rm u}$, once the accretion halts (e.g., Brown et al. 1998; Colpi et al. 2001). Here, $Q_{\rm nuc} \sim 2$ MeV is the nuclear energy deposited per accreted baryon (Gupta et al. 2007; Haensel & Zdunik 2008), $m_{\rm u}$ is the atomic mass unit and $\langle \dot{M} \rangle$ is the time-averaged accretion rate of the system. The latter can be expressed as $\langle \dot{M} \rangle = \langle \dot{M}_{\rm ob} \rangle \times t_{\rm ob}/t_{\rm rec}$, where $\langle \dot{M}_{\rm ob} \rangle$ is the average accretion rate during outburst episodes, $t_{\rm ob}$ is the outburst duration and $t_{\rm rec}$ is the system's recurrence time. The factor $t_{\rm ob}/t_{\rm rec}$ represents the duty cycle of the system.

The outburst of EXO 0748–676 started between 1980 May and 1984 July (see Section 1) and the system returned to quiescence in 2008 September, i.e., $t_{\rm ob} = 24 - 28$ years. The estimated average bolometric flux during outburst is $\sim (7 - 8) \times 10^{-10}$ erg cm^{-2} s^{-1} (Sidoli et al. 2005; Boirin et al. 2007). For an accretion luminosity of $L_{\rm acc} = (GM_{\rm NS}/R_{\rm NS})\langle \dot{M}_{\rm ob} \rangle$, this translates into a mass-accretion rate of $\langle \dot{M}_{\rm ob} \rangle \sim 3 \times 10^{16}$ g s^{-1} for a canonical neutron star with $M = 1.4$ M$_\odot$ and $R = 10$ km (assuming a distance of $D = 7.4$ kpc).[2] As argued above, EXO 0748–676 might already be close to reaching its quiescent base level. To explain a quiescent bolometric luminosity of $\sim 6 \times 10^{33}$ (D/7.4 kpc)^2 erg s^{-1} (as measured during the *Chandra* observation of 2010 April) in terms of thermal emission resulting from deep crustal heating (i.e., opposed to continued accretion), it requires that EXO 0748–676 has a duty cycle of ~ 10 percent. This would imply an expected recurrence time of $\sim 200 - 250$ years if the observed outburst is typical for the long-term behaviour of this source.

Brown et al. (1998), Rutledge et al. (2000) and Colpi et al. (2001) have suggested that EXO 0748–676 continues to accrete in quiescence, because the quiescent luminosity inferred from the 1980 *EINSTEIN* observation is higher than predicted by standard cooling models. However, these conclusions are based on an assumed duty cycle of ~ 1 percent, but we have no a priori knowledge about this. Although we cannot exclude that the system is indeed accreting in quiescence, the above estimates show that a duty cycle of ~ 10 percent (which is not uncommon for neutron star transients) can explain the observed quiescent level of EXO 0748–676 as being due to thermal emission resulting from deep crustal heating.

Recently, Brown & Cumming (2009) demonstrated that the cooling of a neutron star crust is expected to follow a broken powerlaw decay. A break is predicted to occur due to a transition in the crystal structure of the crust matter, and the slope before the break reflects the heat flux from the outer crustal layers. Therefore, we also fitted the neutron

[2] We note that EXO 0748–676 is an eclipsing system and therefore part of the central X-ray flux may be intercepted from our line of sight. However, the X-ray burst behaviour of the source is consistent with the mass-accretion rate inferred from the observed X-ray luminosity (Boirin et al. 2007).

star temperatures obtained for EXO 0748–676 to a powerlaw and found decay indices of -0.03 ± 0.01 and -0.05 ± 0.01 for the *Chandra* and *Swift* data sets, respectively. The *Swift* observations indicate that a possible break in the quiescent lightcurve may have occurred $\sim 67-265$ days after the cessation of the outburst (see Section 3.2). By fitting a broken powerlaw function, we obtain a decay index of -0.03 ± 0.03 before the break, which steepens to -0.06 ± 0.02 thereafter. However, further observations are required to confirm that a break has indeed occurred.

The decay parameters that we find for EXO 0748–676 are comparable to that obtained by Fridriksson et al. (2010) for XTE J1701–462. These authors found that the quiescent lightcurve breaks $\sim 20-150$ days post-outburst and report decay indices of ~ -0.03 and ~ -0.07 before and after the break, respectively. Fridriksson et al. (2010) note that possible cross-calibration effects between *Chandra* and *XMM-Newton* might introduce small shifts that also allow a single powerlaw decay with slope ~ -0.05. The cooling curves of KS 1731–260 and MXB 1659–29 appear to have steeper decays with indices of ~ -0.12 and ~ -0.33, respectively (Cackett et al. 2008). Due to the scarcity of data points it is unclear whether a break occurred in the quiescent lightcurves of those two sources (Cackett et al. 2008; Brown & Cumming 2009).

The powerlaw fits show no indications that the quiescent lightcurve of EXO 0748–676 is levelling off. Thus, it is also possible that the neutron star temperature continues to decay further and that the core is cooler than suggested by the exponential decay fits. The relatively slow decrease of EXO 0748–676 might then reflect that the crust has a high conductivity, albeit lower than that of the neutron stars in KS 1731–260 and MXB 1659–29. Further observations are thus required to determine whether the neutron star crust in EXO 0748–676 has nearly cooled down and to be able to draw conclusions on the crust and core properties.

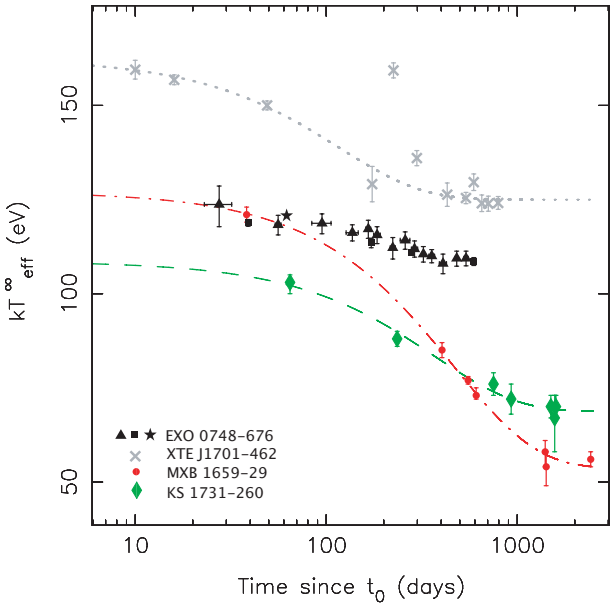

Figure 6. The effective temperatures of KS 1731–260 (green diamonds; from Cackett et al. 2006), MXB 1659–29 (red bullets; from Cackett et al. 2006, 2008), XTE J1701–462 (grey crosses; from Fridriksson et al. 2010) and EXO 0748–676 (black). Exponential decay fits to the data of KS 1731–260, MXB 1659–29 and XTE J1701–462 are shown to guide the eye (green dashed, red dashed-dotted and grey dotted line, respectively). The two data points of XTE J1701–462 that lie above the decay curve are likely due to a temporal increase in the accretion rate onto the neutron star, causing reheating (Fridriksson et al. 2010).

ACKNOWLEDGMENTS

This work was supported by the Netherlands Organization for Scientific Research (NWO) and made use of the *Swift* public data archive. We acknowledge *Swift* PI N. Gehrels and the *Swift* planning team for their help in carrying out the ToO campaign. EMC was supported by NASA through the Chandra Fellowship Program. MTW, PSR and KSW acknowledge the United States Office of Naval Research. JH and WHGL acknowledge support from Chandra grant GO8-9045X.

REFERENCES

Altamirano D., Wijnands R., Degenaar N., Casella P., Homan J., Belloni T., Campana S., 2007, ATel, 1178
Asai K., Dotani T., Mitsuda K., Hoshi R., Vaughan B., Tanaka Y., Inoue H., 1996, PASJ, 48, 257
Bassa C. G., Jonker P. G., Steeghs D., Torres M. A. P., 2009, MNRAS, 399, 2055
Boirin L., Keek L., Méndez M., Cumming A., in't Zand J. J. M., Cottam J., Paerels F., Lewin W. H. G., 2007, A&A, 465, 559
Brown E. F., Bildsten L., Rutledge R. E., 1998, ApJ Lett, 504, L95
Brown E. F., Cumming A., 2009, ApJ, 698, 1020
Cackett E. M., Wijnands R., Linares M., Miller J. M., Homan J., Lewin W. H. G., 2006, MNRAS, 372, 479
Cackett E. M., Wijnands R., Miller J. M., Brown E. F., Degenaar N., 2008, ApJL, 687, L87
Cackett E. M., Brown E. F., Miller J. M., Wijnands R., 2010, submitted to ApJ
Campana S., 2003, preprint (astro-ph/0311212)
Campana S., Colpi M., Mereghetti S., Stella L., Tavani M., 1998, A&ARv, 8, 279
Chen W., Shrader C. R., Livio M., 1997, ApJ, 491, 312
Colpi M., Geppert U., Page D., Possenti A., 2001, ApJL, 548, L175
Degenaar N., et al., 2009, MNRAS, 396, L26
Eichler D., Cheng A. F., 1989, ApJ, 336, 360
Evans P. A., et al., 2007, A&A, 469, 379
Fridriksson J. K., et al., 2010, ApJ, 714, 270
Galloway D. K., Muno M. P., Hartman J. M., Psaltis D., Chakrabarty D., 2008, ApJS, 179, 360
Garcia M. R., Callanan P. J., 1999, AJ, 118, 1390
Gottwald M., Haberl F., Parmar A. N., White N. E., 1986, ApJ, 308, 213
Gupta S., Brown E. F., Schatz H., Möller P., Kratz K.-L., 2007, ApJ, 662, 1188
Haensel P., Zdunik J. L., 1990, A&A, 227, 431
Haensel P., Zdunik J. L., 2003, A&A, 404, L33
Haensel P., Zdunik J. L., 2008, A&A, 480, 459

Heinke C. O., Jonker P. G., Wijnands R., Deloye C. J., Taam R. E., 2009, ApJ, 691, 1035
Heinke C. O., Rybicki G. B., Narayan R., Grindlay J. E., 2006, ApJ, 644, 1090
Homan J., Wijnands R., Altamirano D., Belloni T., 2007, ATel, 1165
Hynes R., Jones E., 2008, ATel, 1816
Hynes R. I., Jones E. D., 2009, ApJL, 697, L14
in't Zand J. J. M., van Kerkwijk M. H., Pooley D., Verbunt F., Wijnands R., Lewin W. H. G., 2001, ApJL, 563, L41
Jonker P. G., 2008, in C. Bassa, Z. Wang, A. Cumming, & V. M. Kaspi eds, 40 Years of Pulsars: Millisecond Pulsars, Magnetars and More, AIP Conf. Ser. Vol. 983, Constraining the neutron star equation of state using quiescent low-mass X-ray binaries. p. 519
Jonker P. G., Galloway D. K., McClintock J. E., Buxton M., Garcia M., Murray S., 2004, MNRAS, 354, 666
Kirsch M. G., Briel U. G., Burrows D., et al. 2005, in Siegmund O. H. W., ed., UV, X-Ray, and Gamma-Ray Space Instrumentation for Astronomy XIV, SPIE Conf. Ser. Vol. 5898, p. 22
Lattimer J. M., van Riper K. A., Prakash M., Prakash M., 1994, ApJ, 425, 802
Parmar A. N., White N. E., Giommi P., Gottwald M., 1986, ApJ, 308, 199
Parmar A. N., White N. E., Giommi P., Haberl F., Pedersen H., Mayor M., 1985, IAU Circ., 4039, 1
Reynolds A. P., Parmar A. N., Hakala P. J., Pollock A. M. T., Williams O. R., Peacock A., Taylor B. G., 1999, AAPS, 134, 287
Rutledge R. E., Bildsten L., Brown E. F., Pavlov G. G., Zavlin V. E., 1999, ApJ, 514, 945
Rutledge R. E., Bildsten L., Brown E. F., Pavlov G. G., Zavlin V. E., 2000, ApJ, 529, 985
Rutledge R. E., Bildsten L., Brown E. F., Pavlov G. G., Zavlin V. E., Ushomirsky G., 2002, ApJ, 580, 413
Shternin P. S., Yakovlev D. G., Haensel P., Potekhin A. Y., 2007, MNRAS, 382, L43
Sidoli L., Parmar A. N., Oosterbroek T., 2005, A&A, 429, 291
Tomsick J. A., Gelino D. M., Halpern J. P., Kaaret P., 2004, ApJ, 610, 933
Torres M. A. P., Jonker P. G., Steeghs D., Seth A. C., 2008, ATel, 1817
Webb N. A., Barret D., 2007, ApJ, 671, 727
Wijnands R., 2004, ArXiv e-prints astro-ph/0405089
Wijnands R., Guainazzi M., van der Klis M., Méndez M., 2002, ApJ Lett, 573, L45
Wijnands R., Homan J., Miller J. M., Lewin W. H. G., 2004, ApJ Lett, 606, L61
Wijnands R., Miller J. M., Markwardt C., Lewin W. H. G., van der Klis M., 2001, ApJ Lett, 560, L159
Wijnands R., Nowak M., Miller J. M., Homan J., Wachter S., Lewin W. H. G., 2003, ApJ, 594, 952
Wolff M. T., Becker P. A., Ray P. S., Wood K. S., 2005, ApJ, 632, 1099
Wolff M. T., Ray P. S., Wood K. S., 2008, ATel, 1736
Wolff M. T., Ray P. S., Wood K. S., Hertz P. L., 2009, ApJS, 183, 156
Wolff M. T., Ray P. S., Wood K. S., Wijnands R., 2008, ATel, 1812
Yakovlev D. G., Levenfish K. P., Haensel P., 2003, A&A, 407, 265
Yakovlev D. G., Pethick C. J., 2004, ARAA, 42, 169
Zampieri L., Turolla R., Zane S., Treves A., 1995, ApJ, 439, 849
Zavlin V. E., Pavlov G. G., Shibanov Y. A., 1996, A&A, 315, 141